Theoretical and Computational Investigations of Carbon Nanostructures

Basant Roondhe, Vaishali Sharma, and Sumit Saxena

Abstract Carbon is one of the most versatile elements in the periodic table and is known to occur in various allotropic forms. It has been widely explored since the eighteenth century and its investigation in various forms has witnessed continuous growth thereafter. The effect of these advancements has guided numerous discoveries which have not only addressed several aspects of materials physics, but also their applications. The development of theoretical and computational tools accompanied by novel characterization techniques along with the ability to synthesize these reduced dimensionalities of the carbon family like fullerene, carbon nanotubes, graphene, carbon quantum dots, etc. has significantly improved the understanding of these nanostructures. The ability of computational and theoretical techniques to predict and provide insights into the structure and properties of systems plays a crucial part in substantiating experimental findings. Theoretical and computational modeling of various carbon nanostructures such as fullerene, carbon nanotubes, graphene, and carbon quantum dots will be critically reviewed. The chapter begins with the description of the historical timeline of carbon nanostructures. How the models developed over time have led to the development of carbon nanoforms is reviewed. The impact of theoretical and computational approaches in understanding the physics of these carbon nanostructures is also highlighted.

Keywords Carbon nanostructures · Theoretical and computational modeling · Fullerene · Carbon nanotubes · Graphene

B. Roondhe · S. Saxena (✉)
Department of Metallurgical Engineering and Materials Science, Indian Institute of Technology Bombay, Mumbai 400076, Maharashtra, India
e-mail: sumit.saxena@iitb.ac.in

V. Sharma
Department of Physics, Faculty of Science, The Maharaja Sayajirao University of Baroda, Vadodara 390002, India

A. Hazra and R. Goswami (eds.), *Carbon Nanomaterial Electronics: Devices and Applications*, Advances in Sustainability Science and Technology,
https://doi.org/10.1007/978-981-16-1052-3_7

1 Introduction

Carbon is one of the essential elements in the world; in terms of abundance, it holds the sixth position of typical elements in the universe, fourth in our solar system, and about seventeenth in the Earth's crust [1]. The approximated relative abundance for carbon ranges 180–270 parts per million [2]. It is also noteworthy that the presence of carbon in human beings as an element is only subsequent to oxygen [3] and therefore acquires around 18% of human body weight. One of the remarkable characteristics of carbon is that it can occur in a broad area of metastable phases modeled near ambient environments along with their extensive kinetic stability. Despite the fact that carbon in its elemental form is relatively scarce on the earth's crust [1, 2, 4], it plays a significant role in the ecosystem of the earth. With the ongoing research toward the development of various unique forms of carbon, the current century can be rightly called "The era of carbon allotropes" [5]. Carbon nanoforms or nanostructures comprise various low-dimensional allotropes such as buckminsterfullerene or C_{60}, carbon nanotubes, graphene, poly-aromatic molecules, and carbon quantum dots. The uses of these nanostructures have been explored in different areas like nanoscience, materials science, engineering, and technology [6–12]. Recently, nanotechnology has gathered much attention because of its direct application in developing novel materials comprising significant properties like better directionality, high surface area with flexibility, etc. [13–18]. These properties uncover various applications of carbon nanomaterials design in almost all research domains [9, 19–23]. Ergo, in recent past decades, carbon science has become a trending topic along with its nanoscience discipline.

Carbon is traditionally understood to occur in only two naturally occurring allotropic configurations known as graphite and diamond. Nevertheless, the crystal structure and properties of graphite and diamond are significantly different [24–28]. Chemically, the tendency of carbon atoms to create covalent bonds with other carbon atoms leads to the formation of novel allotropes in the carbon family [29] such as buckminsterfullerene [30, 31], carbon nanotubes [32, 33], and graphene [11]. Although the existence of carbon and its applications has been known to us for centuries, the modern timeline for the development of carbon science is represented in Fig. 1.

A new chapter in the exploration of the carbon family began with the discovery of buckminsterfullerene's ("buckyballs") [30] in the mid-1980s accompanied by the discovery of fullerene nanotubules ("buckytubes") [33]. The breakthrough discovery of these nanostructures triggered increased research efforts in the exploration of carbon materials. Table 1 presents some predictions and discoveries of carbon nanostructures.

The theoretical and computational approach has made significant contributions in the field of carbon nanostructures (graphene, fullerenes, and carbon nanotubes) by offering a framework with predictive structures along with their chemical and physical properties. Computational framework in nanoscience has consistently complemented the experiments for the development of carbon nanostructures with the

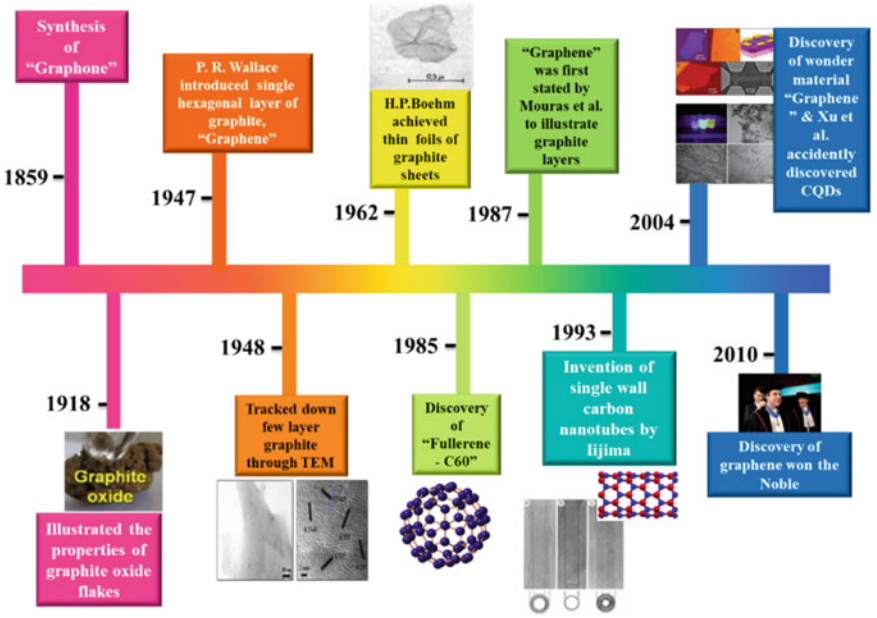

Fig. 1 Timeline of carbon nanostructures

Table 1 Timeline of predictions, discoveries, and observations of carbon nanostructures

Years	Occurrence	Observations
1966	Graphite molecules with hollow-shell were described	Assumption of molecule shape by graphite is made by Jones [34]
1970	A soccer ball-shaped C_{60} molecule is suggested	Osawa [35]
1973	Prediction of stable C_{60} was described	Huckel calculations; closed-shell electronic structure is expected by Bochvar and Galperin [36]
1980	Nanotubes were first observed	Using arc discharge method by Iijima [37]
1985	After several hypotheses, Buckminsterfullerene, C_{60} was discovered	Kroto, Smalley et al. detected C_{60} and C_{70} in the mass spectrum of laser-evaporated graphite [30]
1991	Prediction of hyperfullerenes was made	Curl and Smalley [38]
1993	Single-wall nanotubes were discovered	Using arc process in the presence of iron and cobalt catalytic particles by Iijima et al. [39] and Bethune [40]
2004	Discovery of Graphene	A monolayer graphene was developed using a Scotch tape technique [41]
2004	Discovery of carbon quantum dots	Fluorescent carbon quantum dots were derived accidentally from single-wall carbon nanotubes (SWCNTs) [42]

prediction of their properties. The theoretical approach also provides an understanding of the reaction and separation mechanisms of carbon nanostructures. Experimental methodologies like X-ray diffraction and nuclear magnetic resonance are used for probing and solving the crystal structure of any material. A computational approach can be used alternatively. Several methodologies were developed to deal with the problem of structure prediction. One prominent and effective model comprises investigating material's crystal structure, energy, and thereby choosing the material with the lowest energy as the "best guess" solution. In this context, various methods have been established. Random crystal structure prediction is an easy way that produces random atomic compositions with optimization to stabilize those compositions (inside the limits of bond lengths) [43]. While random crystal structure prediction is simplistic, unbiased, and easy to parallelize, it necessitates sampling various configurations to achieve better results. Another widespread approach to improve efficiency is evolutionary algorithms [44], which initially starts with a random structure and then enriches guesses with the lowest-energy results with each iteration [45]. In order to improve the results of structural prediction, different algorithms, force statistics, and data mining [46–50] are used to study criteria for crystallization such as in the Inorganic Crystal Structure Database [51]. However, the drawback of data mining methodology is that it is identified by the compounds analogous to previously observed ones, hence, lacking in novel and distinct structural phases. The recent approach for efficient crystal structure prediction involves partial experimental information to apply limitations on symmetry [52]. Every method has its own significance for different applications.

To accomplish electronic structure calculations of carbon nanostructures like fullerenes and model CNTs, many-body empirical potentials, empirical tight-binding molecular dynamics, and local density functional (LDF) means were utilized at beginning of the past decade [53, 54]. The Huckel approximation was used to investigate electronic structure for large I_h point group fullerenes [55]. The geometry optimizations of these large fullerenes were also carried by methodologies like molecular mechanics (MM3), semi-empirical methods [56], AM1 [57], PM3 [58], and Semi-Ab Initio Model 1 (SAM1) [59]. The computational strength has also been extensively evolving due to the availability of more powerful computing resources. Consequently, theoreticians are delighted in examining and developing carbon nanostructures past molecular mechanics and semi-empirical methods. An analysis of theoretical and computational approaches utilized to explore different nanostructures of the carbon family is provided in this chapter.

2 Zero Dimensional (0D) Carbon Nanostructures

2.1 Fullerenes

Fullerenes form a hollow cage-like arrangement of carbon atoms comprising solely of hexagon and pentagon rings. Buckminsterfullerene (C_{60}) was the first in the series of developments of such carbon nanostructures [30]. Kroto, Curl, and Smalley were awarded the Nobel Prize in Chemistry in 1996 for this discovery. However, before the experimental realization of these fullerenes, they were first hypothesized by many researchers. In 1966, graphite molecules with hollow-shell were described in the scientific column "Daedalus" [34]. Subsequently, various theoretical hypotheses were made on the capability of 60 carbon atoms with truncated icosahedron [35, 36, 60, 61]. The occurrence of C_{60} was primarily predicted by Osawa in 1970 [35]. These results were later confirmed by mass synthesis of C_{60} by Krätschmer in 1990 using the carbon arc method accompanied by infrared (IR) spectroscopy for structure verification [62]. The aforementioned findings since then sparked widespread novel research for C_{60} along with other fullerene derivatives.

The study for fullerene with the early graphite laser vaporization was initiated and observed by Rohlfing et al. [63]. The carbon clusters formed in the experiments were noticeably bimaximal comprising of even and odd forms of C_n (where $n <= 25$), while only even forms in C_n (where $n >= 40$) relying upon their experimental situations. According to ab initio and various spectroscopic investigations, carbon clusters varying from $n = 2$ to 9 tend to present linear chain structures with single and triplet electronic ground states in odd and even clusters, respectively [63]. Contrary to that, some ab initio studies suggest that even number clusters in the range $n = 2$–8 show cyclic equilibrium structures with lower electronic states [64, 65]. Furthermore, C_n clusters ranging from $n = 10$ to 25 present monocyclic ground state configurations. The above-said conversion from linear chains to monocyclic rings is attributed to the fact that additional bonding associated with ring closure ultimately surpasses the strain energy acquired with the twisting of the polyyne chain to create a ring. Through semi-empirical molecular orbital theory calculations, the transformation point with 10 carbon atoms is predicted [66, 67]. However, according to the intensities in the high-mass region, these carbon nanostructures were indecisive and needed plausible explanations [68]. The photoionization time-of-flight mass spectrum (PI-TOF-MS) of these carbon nanostructures ranging from 1 to 100 atoms is presented in Fig. 2.

Evidently, these elucidations must justify the detail that ion signals of even C_n were observed in the high-mass region. Subsequently, this instantly eliminates a variety of probable configurations for $C_n$clusters, for instance, fractions of diamond lattice/graphite sheet. These structures tend to present both even and odd peaks of mass by means of linear chains and monocyclic rings. Moreover, it does not exclude the possibilities of other configurations like "carbyne" [63]. The second probable reason consistent with this analysis would be that the second sets of high-mass region carbon clusters are all fullerenes (Fig. 2). This is the well-known fullerene hypothesis and has gathered much attention for the reason that closed cages bypass

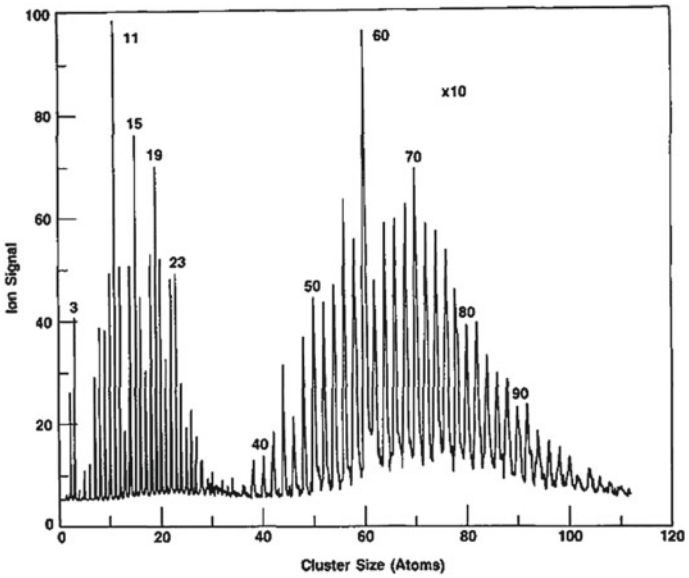

Fig. 2 PI-TOF-MS spectrum (involving the amalgamation of two different spectra) for carbon clusters attained through doubled Nd:YAG vaporizing laser energy (40 mJ) and unfocused ArF ionizing laser energy (1.6 mJ and 193 run). The vertical deflection plate voltage of 300 V is utilized for C_n^+, $1 < n < 30$, leading to the optimization of C_{20}^+ collection while 600 V was utilized for C_{2n}^+, $20 < n < 50$, for the optimization of C_{100}^+. Reproduced with permission from Rohlfing et al. J. Chem. Phys 81, 3322 (1984). Copyright 1984 AIP Publishing

the dangling bonds of edges that are anticipated to destabilize fractions of diamond and graphite lattices [30] and additionally, due to the fact that trivalent cages fulfill the valence necessities of carbon atoms compared to linear chains and monocyclic rings. These qualitative theoretical aspects of the fullerene hypothesis along with electronic structure calculations provided support to the experimentation of C_{60} in 1985.

One of the important investigations performed was the comparison of carbon cages with chains, rings, and toroids along with fractions of infinite diamond and graphite lattices using semi-empirical models [69]. The analysis suggested that cage structures with atoms greater than 25 would be the most stable carbon clusters. Furthermore, the existence of solely pentagonal and hexagonal rings along with the unavailability of adjacent pentagonal rings were conditions for the stability of cage structures [69]. The affinity of fullerenes comprising limited adjacent pentagonal rings was also addressed by Kroto in 1987 using empirical arguments derived from chemical and geodesic rules [70]. The structures studied by Kroto in 1987 are presented in Fig. 3. It is noteworthy that both the aforementioned studies suggested that C_{60} was the smallest fullerene without adjoining pentagonal rings consists of D_{5h} isomer of C_{70}.

Kroto's inference of C_{60} with I_h symmetry as foundational fullerene was supported by Krätschmer et al. [62] in 1990 through four-band IR absorption spectrum and

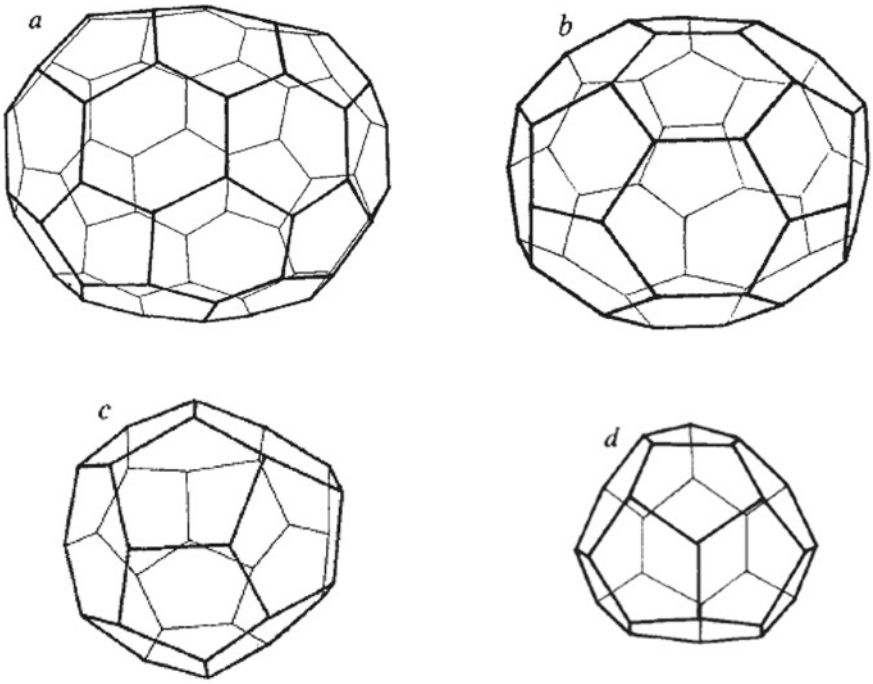

Fig. 3 Structures of fullerenes by Kroto et al. **a** C_{70}, most stable fullerene created by splitting two halves of C_{60} through 10 extra carbon rings, **b** C_{50}, comprising isolated singlet and doublet pentagonal structures, **c** structure of C_{32} with threefold axis, and **d** C_{28} which is a tetrahedral fullerene. Reproduced with permission from Kroto, Nature 329, 529 (1987). Copyright 1987 Springer Nature

latterly in the same year by Taylor et al. [71] through ^{13}C nuclear magnetic resonance (NMR) spectroscopy. Thereafter, several other configurations of fullerenes were synthesized including C_{76} [72], C_{78} [73, 74], and C_{84} [74, 75].

Various configurations of fullerenes are shown in Fig. 4. Each fullerene molecule shows the features of a carbon cage, as each atom is bonded to the other three carbon atoms in the same manner as in graphite [73]. The extensive series of techniques to synthesize fullerenes observed that C_{60} is the most plenteous among fullerenes accompanied by C_{70} [76]. C_{60} with I_h symmetry comprises two C–C bonds with (i) one at the link of two hexagonal rings denoted and (ii) one at the link of pentagonal and hexagonal rings. Contrarily, C_{70} with D_{5h} symmetry consists of eight C–C bonds. It is noteworthy that two pentagonal rings sharing similar C–C bonds are energetically unfavorable. Mathematically, 1812 methods are known to build isomers of 60 carbon atoms, while C_{60} holds its uniqueness and special place with stability due to the fact that all of its pentagonal rings are secluded by its hexagonal rings. The state is known as the "isolated pentagon rule" (IPR) [77]. C_{60} being the smallest member of fullerene family obeying the IPR, C_{62}, C_{64}, C_{66}, and C_{68} fullerenes does not follow the IPR.

Figure 5 presents that the number of IPR isomers is directly proportional to the

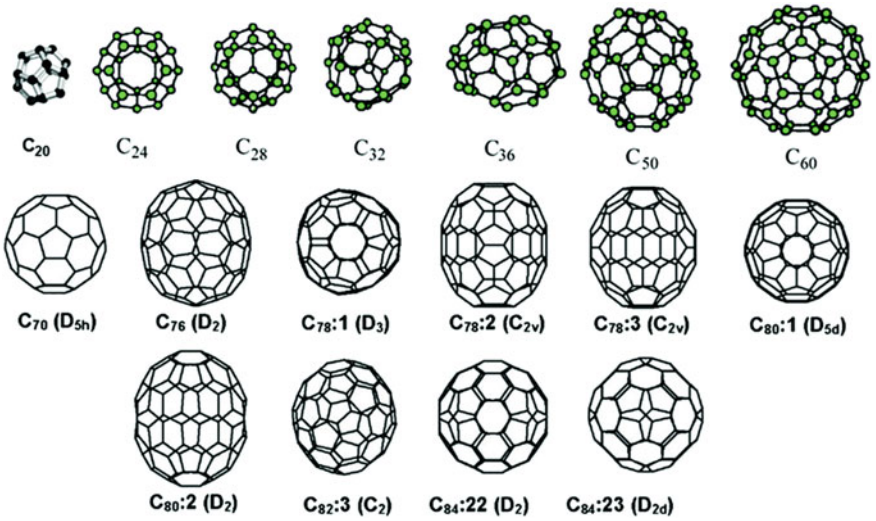

Fig. 4 Structures of fullerenes along with their symmetries. Reprinted with permission from Ref. [73]. Reproduced with permission from Yan et al. Nanoscale 8, 4799 (2016). Copyright 2016 Author(s), licensed under the Creative Commons Attribution 3.0 Unported License

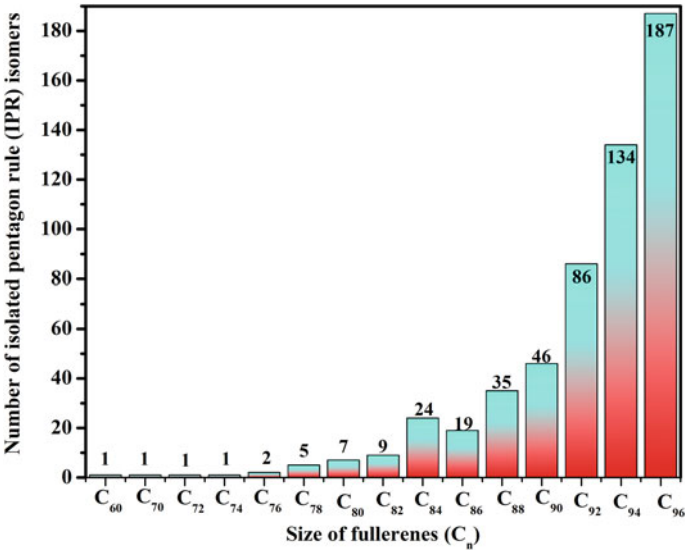

Fig. 5 Size of fullerenes with respect to the number of isolated pentagon rule (IPR) isomers (the details of isomers were taken from Ref. [77])

size of fullerenes. The studies of IPR with possible isomers of fullerenes assisted the experimentalists to identify and characterize them [78–80]. For instance, in C_{78} (consisting five isomers), isomers with C_{2v} and D_3 symmetry were identified using ^{13}CNMR spectra [74]. Theoretical investigations of C_{82} lead to experimental characterization of its three isomers having C_2 symmetry also using ^{13}C NMR spectra [74, 81]. Additionally, several computational investigations were performed since the discovery of fullerenes to thoroughly study their isomers and subsequently to predict the lowest-energy configurations of giant fullerenes [82–89]. Becke, 3-parameter, Lee–Yang–Parr(B3LYP)hybrid functional along with various basis sets were used to examine C_{86} along with its 19 isomers following IPR [87]. Their studies suggested that isomer 17 (C_2 symmetry of C_{86}) is the most stable among them followed by isomer 16 (C_s symmetry of C_{86}). Similarly, several theoretical calculations played a crucial role in predicting accurate lowest-energy structures of the fullerene family [83, 87].

Several theoretical and computational studies in the last decades have been dedicated to exploring C_{60} along with its chemical and physical properties. Theoretical investigations by Fowler and Steer [90] suggested that C_n (n = 60 + 6 k, k = an integer except one) should comprise closed-shell electronic structures. Schmalz et al. showed that the aromaticity of C_{60} is less than that of benzene [69] through resonance circuit theory and Huckel molecular orbital (HMO) theory. The stability occurring through bond delocalization was explained by Amic and Trinajstic [91]. The electronic and vibrational properties of C_{60} were evaluated through the two-dimensional HMO method [92]. Semi-empirical calculations involving overlapping of non-planar π-orbital were also given by the free-electron model in the Coulson–Golubiewski, self-consistent Huckel approximation for the curvature system [93]. The large-scale restricted Hartree–Fock calculations were carried out presenting electron affinity of 0.8 eV and ionization potential to be 7.92 eV with ΔH_f = 415–490 kcal/mol [94–96]. On the basis of ab initio self-consistent field (SCF) theory, the heat of formation was also evaluated by Schulman and Disch [97]. To measure structural parameters, electronic spectra, and oscillator strength, the Pariser–Parr–Pople method and the CNDO/S method (with CI) were used by many researchers [98–101]. The ground and excited states of C_{60} presenting π-bonding character were determined by the tight-binding model using electron–phonon coupling [102]. The primarily vibrational properties of C_{60} were investigated by Newton and Stanton using MNDO theory [103]. It was observed that C_{60} contains four IR active modes because of its high symmetry ("t_{1u}" symmetry) and 10 Raman active modes involving eight "h_g" and two "a_g" symmetries. The 174 vibrational modes of C_{60} contribute to 42 elementary modes with different symmetries. Proceeding to understand magnetic properties of C_{60}, by means of HMO and London theories, the ring current magnetic susceptibility was evaluated with less than 1 ppm shielding because of the termination of the contribution of both diamagnetic and paramagnetic spins [104, 105]. The theory also presented the absence of usual aromatic behavior [104, 105]. Some investigations proposed that the diamagnetic part has been underestimated [106]. Fowler et al. (using coupled Hartree–Fock calculations) in their study proposed that the aforementioned shielding has to be approximately similar as for analogous aromatic structures

[106]. Later on, Haddon and Elser addressed the shielding of fullerenes [104, 105, 107] and reinterpreted the study done by Fowler et al. [106], concluding that their study is inconsistent with the results of small delocalized susceptibility. The chemical shift observed in NMR analysis of C_{60} done by Taylor et al. indicated the presence of aromatic systems; these were confirmed by Fowler and group subsequently [71].

Several theories and computational studies have also been dedicated to exploring doping, defects, functionalization, etc. in fullerenes for their possible applications in antiviral activity, DNA cleavage, photodynamic electron transfer, lightweight batteries, lubricants, nanoscale electrical switches, cancer therapies, and astrophysics [109, 110].

2.2 Carbon Quantum Dots

Carbon quantum dots or carbon dots are relatively newer members among the carbon nanostructure family. These are quasi-spherical nanoparticles involving sp^2/sp^3 amorphous or nanocrystalline forms having size generally <10 nm carrying oxygen/nitrogen groups [111, 112]. Surprisingly, carbon dots were discovered unintentionally in 2004 in an experimental study of carbon nanotubes through electrophoretic fractionation of arc-discharge soot [42]. Carbon dots have gained much attention due to the fact that they possess strong fluorescence with better solubility, biocompatibility, and non-toxicity [113]. However, these fluorescent carbon nanostructures gained significant attention due to improved fluorescence emissions through the surface passivation synthesis approach [114]. The carbon quantum dots along with their STEM and absorption spectra are shown in Fig. 6.

Experimental and theoretical investigations have been used to understand the chemical and physical properties of carbon quantum dots for their applications in various fields like sensing, bio-imaging, nano-medicine, catalysis, optoelectronics, and energy conversion/storage. However, there are considerably rare theoretical studies on carbon quantum dots, and many of them are based on the graphene nanoflakes model [115–120].

Analogous to other quantum dots, the emission of carbon quantum dots is associated to their respective sizes. Carbon quantum dot size <1.2 nm showed UV light emission [121], visible light emissions were reported for quantum dots with size from 1.5 to 3 nm while near-infrared emissions were observed for quantum dots with sizes ~3.8 nm [122]. These observations have also been supported using theoretical calculations. The observation of indirect dependence of the HOMO–LUMO gaps on the size of the carbon quantum dots lead to the conclusion that strong emission of carbon quantum dots is a result of its quantum size rather than carbon–oxygen surface [123]. The photoluminescence mechanism, electronic structures, and frontier molecular orbitals of carbon quantum dots have also been studied using time-dependent density functional theory (TD-DFT) as implemented in Gaussian 09 with B3LYP hybrid functional and the 6-31G(d) basis set [124]. The carbon quantum dots were categorized in two forms: class I representing graphitized carbon core and class II

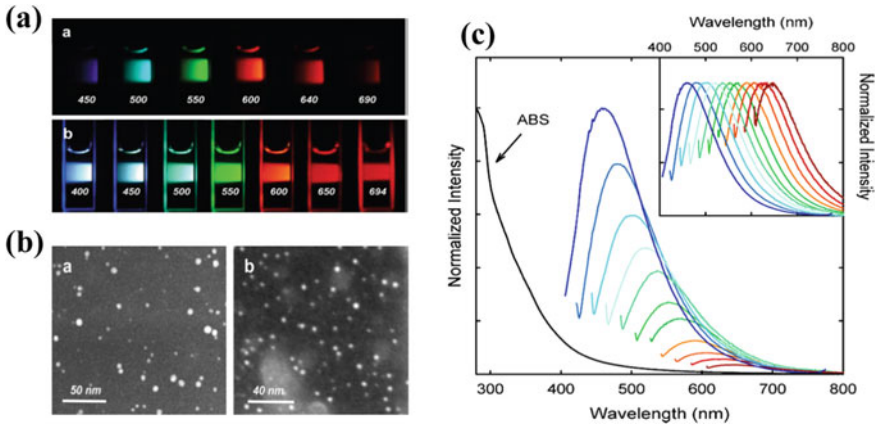

Fig. 6 **a** Carbon dots attached with PEG1500N in aqueous solution. **b** STEM images of carbon dots. **c** The absorption (ABS) and luminescence emission spectra of carbon dots in an aqueous medium; the graph is plotted with 20 nm increment from longer excitation wavelengths 400 nm on the left and the intensities of emission spectral are normalized to quantum yields (inset is the normalized spectral peaks). Reproduced with permission from Sun et al., J. Am. Chem. Soc. 128, 7756 (2006). Copyright 2006 American Chemical Society

representing disordered carbon core. These classes are depicted in Fig. 7 along with their photoluminescence mechanism.

The study showed that the HOMO–LUMO gap decreases with an increase in the size of class I carbon quantum dots while an opposite trend on the size-dependency of the HOMO–LUMO gap is observed for class II carbon quantum dots. Several studies related to the electronic structure of carbon quantum dots have been explained using molecular orbital (MO) theory [121, 123, 125–127]. In the majority of these reports, carbon quantum dots show $n \rightarrow \pi^*$ and $\pi \rightarrow \pi^*$ transitions because of their well-available transition energies. The π-states of carbon quantum dots are attributed to the sp^2 hybridized carbon in their core, while the n-states are attributed to the functional groups attached. It is found that the energy gap (E_g) among π-states reduces consistently with the increase in the number of aromatic rings of carbon quantum dots similar to organic molecules [121, 123]. The electronic properties of amorphous carbon nanodots were explored using semi-empirical molecular–orbital theory using the EMPIRE13 code [128]. Unexpectedly, electronic structures were found to rely weakly on parameters like elemental composition and atomic hybridization. Contrarily, the geometry of sp^2 arrangement describes the band gap of carbon quantum dots. The existence of localized electronic surface states resulting in amphoteric reactivity and near-UV/visible range optical band gaps was predicted [128]. The molecular orbitals, molecular electrostatic potential (MEP), local electron affinity (EA_L), and ionization energy (IE_L) maps along with excitation energies are depicted in Fig. 8. There have been fewer theoretical studies to understand their optical and electronic mechanisms and in-depth theoretical studies are further expected.

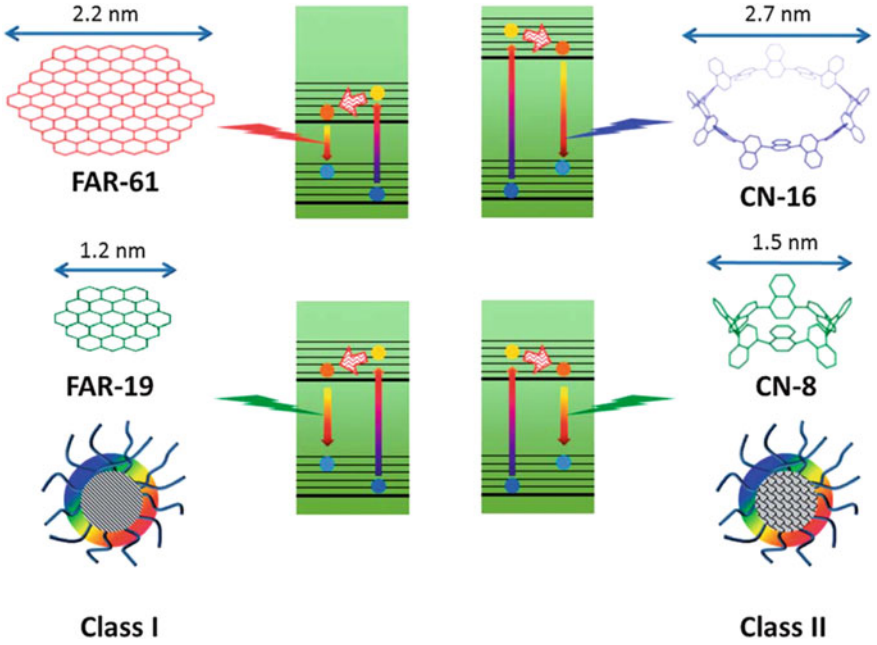

Fig. 7 Photoluminescence (PL) mechanism of class I and class II carbon quantum dots. The number of hexagonal rings is indicated after fused aromatic rings (FARs) and the number of repeating units of cyclo-1,4-naphthylene (CN) is indicated by a number. Reproduced with permission from Zhu et al., J. Mater. Chem. C 1, 580 (2013). Copyright 2013 Royal Society of Chemistry

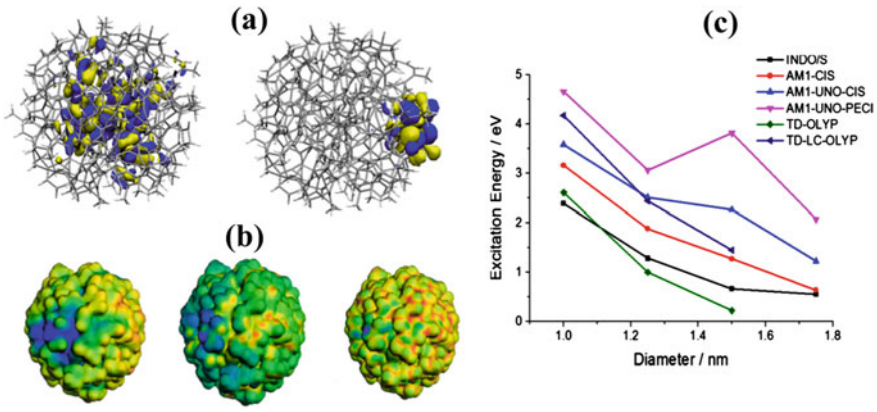

Fig. 8 A 2 nm carbon dot with **a** molecular orbitals; left side presents band-like and right side presents surface states with iso-density surfaces of 0.01 e^{-} Å^{-3}. **b** Electron iso-density surface maps, MEP (left part) from −50 (blue) to 50 kcal mol^{-1} (red), EA_L (middle part) from −150 (blue) to 5 kcal mol^{-1} (red) and IE_L (right part) from 270 (blue) to 500 kcal mol^{-1} (red). **c** Excitation energies calculated with different methods for different sized carbon dots. Reproduced with permission from Margraf et al., J. Phys. Chem. B 119, 24, 7258 (2015). Copyright 2015 American Chemical Society

3 One Dimensional (1D) Carbon Nanostructures

The first-ever proof for the existence of one-dimensional carbon allotrope was reported in 1993 [40]. Single-walled carbon nanotubes (SWCNT) discovered by Iijima and Bethune lead all scientists for a hunt to utilize this a new form of carbon in many applications for technological advancement like field emission displays, energy storage and energy conversion devices, sensors, hydrogen storage, and semiconductor devices [129–134].

CNT is one of the exceptional inventions which has enriched the field of nanotechnology. It has been consistently studied since the past 20 years due to its potential application in varied areas. The fullerenes discovered by Kroto et al. [30] were the building blocks of the CNTs. CNTs have a variety of physical properties such as stiffness, elasticity, deformation, and tensile strength along with electronic properties showing superconducting, metallic, semiconducting, or insulating behavior.

The discovery of CNTs was reported as a "worm-like" structure long before this tubular form of carbon could be imagined, in 1952 by Radushkevich and Lukyanovich [135]. Dimensionally, SWCNTs are around 1 nm in diameter while their length is in order of a few micrometres. Nevertheless, the size and the shape of nanotubes can vary. The ratio of the diameter and length of the nanotubes, also known as aspect ratio, is typically around 1000 due to which it is generally considered nearly as a one-dimensional structure [136].

The different types of CNTs depend on the number of carbon layers present in them. Monolayered tubes are called single-walled carbon nanotube (SWCNT), while tubes having more than one layer are known as multi-walled carbon nanotubes (MWCNTs). The SWCNTs are generally understood to form by rolling a graphene sheet. Density functional theory calculations have shown the possibility of forming CNTs from bilayer graphene nanoribbons under different pressure conditions depending on the edges of nanoribbons involved [137]. The CNTs are classified into three different types: armchair, zigzag (see Fig. 9), and chiral carbon nanotubes (see Fig. 10). These are formed by rolling graphene sheets along a different axis. The axis of rolling is the chiral vector which is represented by n and m pair (n, m) of indices corresponding to the unit vectors along different directions in the graphene honeycomb crystal lattice sheet. When m = 1, 2,… and n = 0, the nanotube is "zigzag" and if m = n, the nanotube is then termed as "armchair" while the remaining configuration iscalled chiral [136, 138, 139]. Due to the rolling of the sheet into a tube, the symmetry of the plane breaks and forms a new symmetry in a distinct direction of the hexagonal lattice and the axial direction. This develops a peculiar electronic behavior of the nanotube, which is metallic or semiconducting. In the case of the semiconducting tube, its bandgap is sensitive toward its diameter; the small diameter tube has a large band gap while the wide diameter consists of a lower band gap [140]. The diameter of the nanotube thus makes it a conductor with conductivity higher than copper as well as a semiconductor comparable to the potential of silicon. In the structure of a nanotube, every carbon atom is bonded covalently with three nearby carbon atoms with its sp^2 molecular orbital, creating one (the fourth) valence electron free in

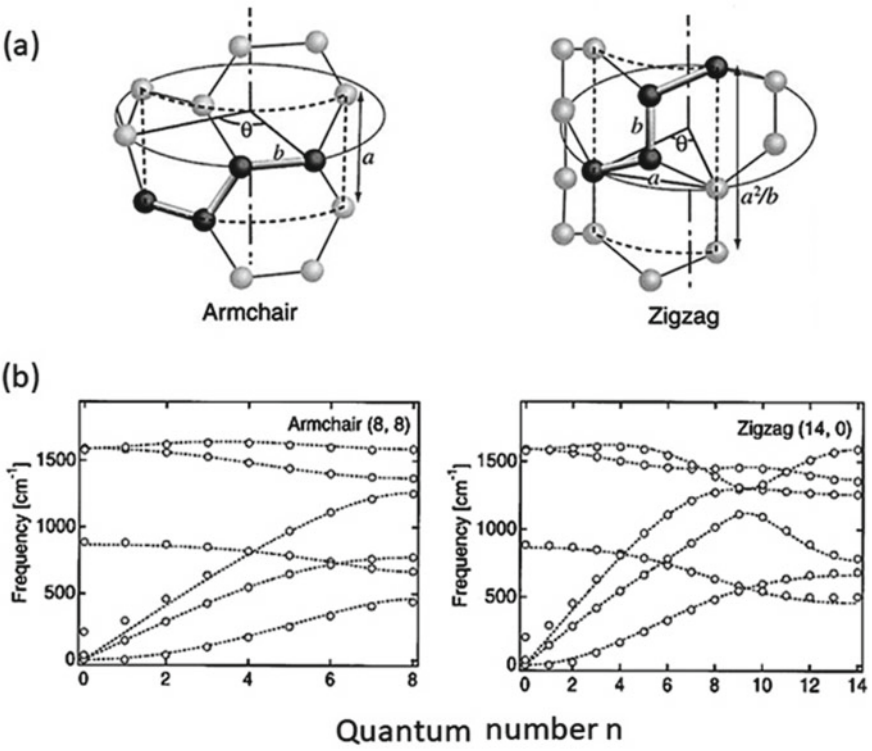

Fig. 9 **a** Unit cell for two different carbon nanotubes (armchair and zigzag) depicting the primitive azimuthal angle θ (=2π/N). **b** Phonon dispersion curve for armchair and zigzag SWCNT. Reproduced with permission from Maeda et al., Physica B 263–264, 479 (1999). Copyright 1999 Elsevier

every hexagonal unit, which is delocalized over all atoms providing the nanotube its electrical nature. Some CNTs which show metallic nature have the resistivity in the range of 0.34×10^{-4} to 1.0×10^{-4} Ω/cm [141]. The semiconducting CNTs generally show p-type semiconducting behavior [142]. The SWCNTs can also be described as quantum wires due to their ballistic electron transport, while the electronic transport in MWCNTs is quasi-ballistic [143]. Apart from the well-known electronic properties of CNTs, they show equally good mechanical properties as well. The sp^2 carbon–carbon bonds present in the CNTs result in exceptional mechanical properties which were not observed in previously explored material systems. From some previous studies, we get an idea about the stiffness of CNTs, basically in their axial direction [144]. Among all carbon materials, CNTs show extremely high value for Young's modulus (~1TPa) which is even five times higher than steel, and provides a measure of the stiffness of the material [145, 146]. All the studies regarding the mechanical properties of CNTs were first predicted theoretically [53, 147–149]. The transformation from the hexagonal ring of carbon to pentagon–heptagon in CNTs

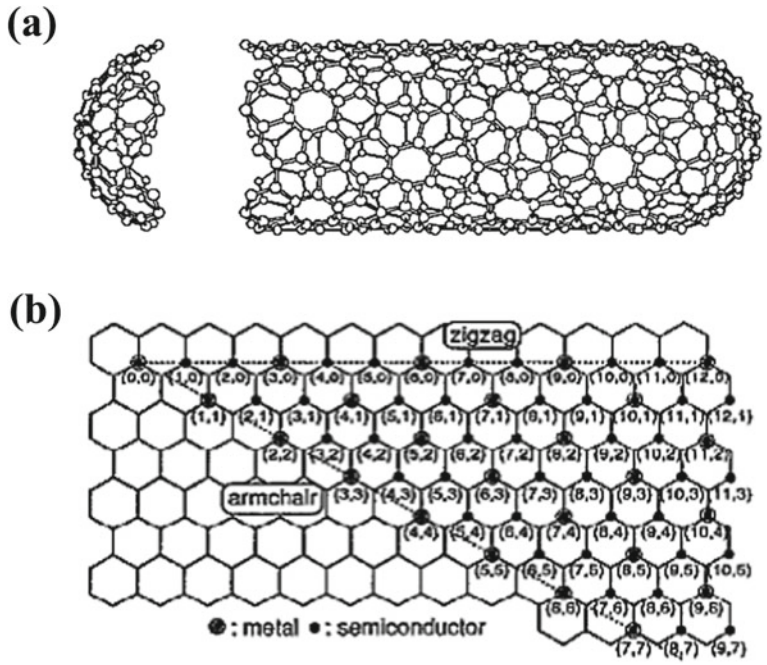

Fig. 10 **a** Icosahedral C_{140} fullerene-based hemispherical cap covered end chiral fiber with chiral vector $C_h = (10, 5)$. **b** Different probable vectors for the construction of chiral fibers. The two different combinations of circled dots and dots denote the metallic and semiconducting behavior for corresponding chiral fiber constructed. Reproduced with permission from Saito et al. Appl. Phys. Lett. 60, 2204 (1992). Copyright 1992 AIP Publishing

was proposed by Yakobson [150] and Ru [151] when uniaxial tension is applied. DFT calculations suggest that SWCNTs form novel quasi-two-dimensional sheets when subjected to high pressure [152]. In a theoretical study done by Guanghua et al. [153] on the CNTs' mechanical properties, their nature of dependence on diameter is revealed. They found Young's modulus in the range of 0.6–0.7 TPa for nanotubes with diameter >1 nm. The closest agreement with the experimental value of Young's modulus of MWCNTs (1–1.2 TPa) was theoretically calculated by Hernandez et al. [154]. In this study, they also predicted that mechanical properties depend on the diameter of the tube; when the diameter increases, the properties are also enhanced to a certain value and ultimately reach the values corresponding to that of graphene. Calculated values of Young's modulus for individual SWNTs were found in the range from 320 to 1470 GPa [144, 155] while the breaking strength ranged from 13 to 52 GPa [156]. The vibrational properties of CNTs are studied by the normal mode analysis as this technique is standard to understand the dynamics of nanotubes. This technique investigates the harmonic potential analytically for normal mode analysis. The linear combination of Cartesian co-ordinates provides the co-ordinates for

normal mode. This method provides a natural description of molecular vibration as it includes the motion of all atoms simultaneously during the vibration.

Apart from the small size, CNTs show quantum effects leading to the low-temperature specific heat and thermal conductivity; CNTs are also of great importance for their thermal properties [149, 157, 158]. The thermal conductivity can be modulated and increased by incorporating different materials with pristine CNTs. The thermal conductivity measured at room temperature for MWCNTs was found to be 3,000 W/K [159], while in a similar study the MWCNTs were found to have thermal conductivities ~200 W/mK higher as compared to the SWCNTs [160]. The main factor which influences the thermal properties is the number of active phonon modes along with a free path of phonon and boundary surface scattering [160–162]. Properties of CNTs are observed to depend on the atomic arrangement, length and diameter of tubes, structural defects, and impurities [163–165].

4 Two-Dimensional (2D) Carbon Nanostructures: Graphene

Graphene is a single atom layer of carbon atoms arranged in a hexagonal honeycomb pattern. It is one of the most studied two-dimensional (2D) materials to date. Figure 11 illustrates a graphene sheet as a 2D building block for different carbon materials in all dimensions such as 0D buckyballs by wrapping up the graphene sheet, 1D nanotube by rolling it, and in 3D graphite by stacking it. Thus, it is known as the mother of

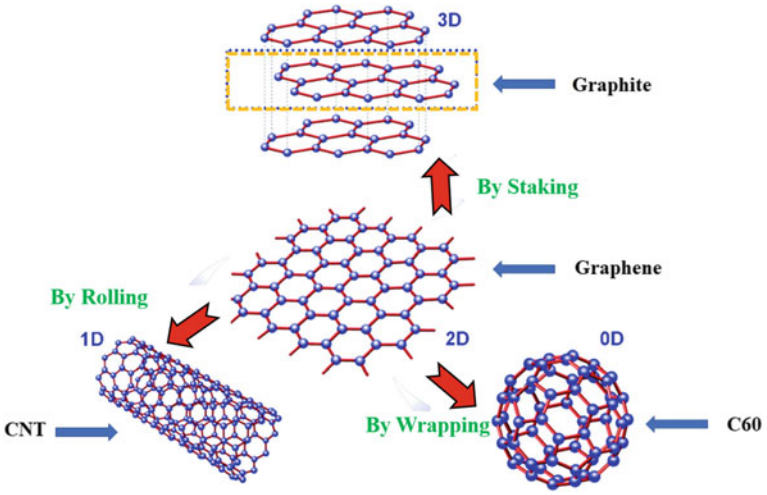

Fig. 11 Graphene sheet is a 2D building block for different carbon materials in all dimensions like 0D buckyballs which is formed by wrapping of graphene sheet, 1D nanotube can be made by rolling it and 3D graphite is formed by stacking it, therefore it is known as the mother of all graphitic forms of carbon material

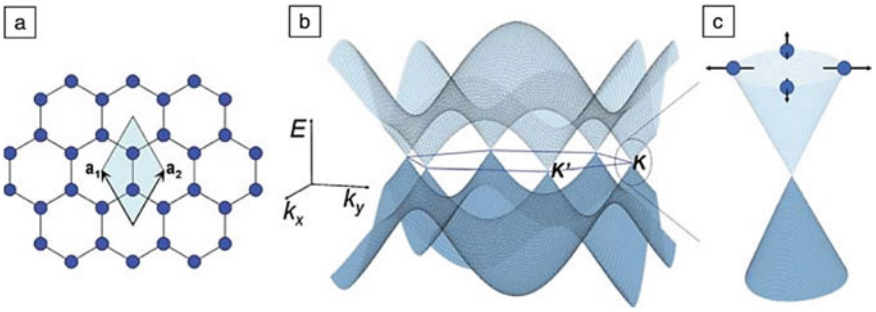

Fig. 12 **a** Unit cell of graphene with the triangular Bravais lattice having lattice vectors a_1 and a_2; unit cell comprises two atoms in the honeycomb lattice. **b** Band structure of graphene calculated by the tight-binding method displaying the pi bands, with only nearest neighbor hopping. The inset E, k_x, and k_y are the energy and the wave vector components in x- and y- directions, respectively. **c** The unique linear dispersion of the band structure near K point with the pseudo-spin vector direction indicated by the arrows. Reproduced with permission from Fuhrer et al. MRS Bulletin 35, 289 (2010). Copyright 2010 Cambridge University Press

all graphitic forms of carbon material. The research has exponentially developed after 2004 when Geim and Novoselov isolated graphene for the first time using the "Scotch Tape" method and characterized it. In the current scenario of the material world, ongoing research is overwhelmed after focusing on characterization, mass production of ultra-thin carbon films including graphene for various applications [166–172].

A unit cell of graphene with the Bravais lattice along with the band structure is shown in Fig. 12. The unique linear dispersion of the band structure near the K point is illustrated by a pseudo-spin direction which is indicated by the arrows. From the past one and half decades, promising applications in the field of corrosion prevention [173], super capacitors [174, 175], long-lasting batteries [176], display panels [177], efficient solar cells [178], desalination [179], and water purification [180–182] have emerged.

The electronic properties of single-layer graphite were investigated by Wallace even before its isolation [183] and introduced the term "graphene" back in 1947. The electronic band structure was investigated theoretically by the tight-binding (TB) approach. The TB approach is more suitable for handling larger systems than the plane waves method, due to its low computational costs. The method was at first described as an interpolation scheme by Slater and Koster [184]. It has been developed comprehensively and now it is a well-established technique to explain the electronic structure of solids [185].

The tight-binding (TB) calculations were performed using the Hamiltonian

$$H = \sum_{il_1\sigma} \epsilon_{l_1} a^{\dagger}_{il_1\sigma} a_{il_1\sigma} + \sum_{ij} \sum_{l_1,l_2,\sigma} \left(t^{l_1 l_2}_{ij} a^{\dagger}_{il_1\sigma} a_{jl_2\sigma} + H.c. \right) \quad (1)$$

here, the spin σ of the electron is capable of jumping from the orbital l_1 with its onsite energies (ϵ_{l_1}) existing in the ith unit cell to orbital l_2 in the jth unit cell. The hopping interaction strength labeled as $t_{ij}^{l_1 l_2}$ relies on the nature of the orbitals participating as well as on the lattice geometry [184]. Following that, a least-squared error fitting is executed through the alteration of the ϵ's and t's, leading to the calculation of band dispersions at various high-symmetry points. Graphite layer shows semiconducting behavior with zero activation energy at zero temperature, but at higher temperatures due to excitation, the highest bands are filled and show metallic nature. Large anisotropic diamagnetic susceptibility which is greatest across the layers is observed. The study done by Boehm in 1962 provided the concept of single-layer graphite sheet through the reduction of graphite oxide (GO) in dilute sodium hydroxide and also by deflagration of heated GO [186]. To describe the atom intercalation in graphite, effective-mass-approximation differential equations were used at that time for self-consistent screening. At room temperature, graphene displays a strong ambipolar electric field effect between the valence and the conduction bands. This results in ballistic electron transfer at a speed which is slower than light speed and 10–100 times greater than that in silicon chips. Graphene is the thinnest material and is 200 times stronger than steel and harder than diamond but at the same time, it is flexible and transparent [10, 187, 188].

Investigation of the physical properties of graphene reveals that it has a tremendously high optical transparency of up to 97.7%, which makes it a potential material for transparent electrodes for its use in solar cell applications [189]. It also consists of high thermal conductivity of 5000 Wm^{-1} K^{-1} [190], and exceptional mechanical properties like high Young's modulus of 1 TPa [191], and most importantly large specific surface area of 2630 m^2 g^{-1} [192]. Still, there is a need to find a method for the utilization of graphene in many applications and also to guarantee cost-effective production by avoiding some major obstacles. It is a great need to develop a method with the help of which ideally flat graphene membrane without any defects can be achieved. The need to fill the large gap between the theoretical prediction and actual fabrication of graphene is essential. Irreversible agglomerates and the restacking are a key challenge in the synthesis of graphene which need to be addressed.

5 Summary and Outlook

Nanomaterials provide exotic properties, exclusive of the framework of their periodic solid counterparts. Additionally, novel phenomena emerge at the nanoscale level that is not observed in microcrystalline materials. Among all, carbon nanostructures like three dimension (3D—Graphite, diamond), two dimension (2D—graphene), one dimension (1D—carbon nanotubes), and zero dimension (0D—fullerenes and carbon quantum dots) have gained significant attention due to their unique properties. The discovery of C_{60} and carbon quantum dots (0D), CNTs (1D), and graphene (2D) has led to the increased research activity in novel multidisciplinary areas, from synthesis

to their theoretical and computational investigations for potential applications. In the present chapter, the theoretical and computational development of carbon nanostructures, specifically on fullerenes, carbon quantum dots, carbon nanotubes, and graphene have been introduced and discussed. The underlying mechanism of size dependency of these carbon cage structures (fullerenes and carbon nanotubes) is essential for modifying their properties according to the potential nanotechnology applications. Computational and theoretical studies have found significant role in predicting and designing their properties accordingly. By the means of powerful supercomputers, performing static and dynamic calculations at high-level ab initio and DFT methodologies is achievable for these carbon nanostructures. Still, the application of futuristic quantum chemical approaches to investigate the structures and properties of large carbon nanostructures (fullerenes, carbon quantum dots, graphene, and CNTs) is a daunting task. The theory of isolated pentagon rule (IRP) in fullerenes chemistry has been discussed. The knowledge on the computational and theoretical aspects of accidentally discovered carbon quantum dots were explored which is still in its developing stage. The theoretical prediction of carbon nanotubes (armchair, zigzag, and chiral) and graphene before their experimental realization is provided. Obtaining insight of the electronic structures along with their chemical and physical properties is still needed for constructing new materials based on carbon-based nanostructures for certain applications. The synergy among theoreticians and experimentalists will expand the applications of carbon nanostructures promptly.

References

1. Zhang Y, Yin Q-Z (2012) Carbon and other light element contents in the Earth's core based on first-principles molecular dynamics. Proc Natl Acad Sci USA 109:19579–19583
2. Allègre CJ, Poirier J-P, Humler E et al (1995) The chemical composition of the Earth. Earth Planet Sci Lett 134:515–526
3. Pace NR (2001) The universal nature of biochemistry. Proc Natl Acad Sci USA 98:805–808
4. Marty B, Alexander CMO, Raymond SN (2013) Primordial origins of Earth's carbon. Rev Mineral Geochem 75:149–181
5. Hirsch A (2010) The era of carbon allotropes. Nat Mater 9:868–871
6. Titirici M-M, White RJ, Brun N et al (2015) Sustainable carbon materials. Chem Soc Rev 44:250–290
7. Loos M (2015) Allotropes of carbon and carbon nanotubes. Elsevier, Amsterdam, The Netherlands
8. Deng J, You Y, Sahajwalla V et al (2016) Transforming waste into carbon-based nanomaterials. Carbon 96:105–115
9. Rodríguez-Reinoso F (1998) The role of carbon materials in heterogeneous catalysis. Carbon 36:159–175
10. Allen MJ, Tung VC, Kaner RB (2010) Honeycomb carbon: a review of graphene. Chem Rev 110:132–145
11. Geim AK, Novoselov KS (2007) The rise of graphene. Nat Mater 6:183–191
12. Novoselov KS, Fal VI, Colombo L et al (2012) A roadmap for graphene. Nature 490:192–200
13. Stankovich S, Dikin DA, Piner RD et al (2007) Synthesis of graphene-based nanosheets via chemical reduction of exfoliated graphite oxide. Carbon 45:1558–1565

14. Zhu Y, Murali S, Stoller MD et al (2011) Carbon-based supercapacitors produced by activation of graphene. Science 332:1537–1541
15. Gadipelli S, Guo ZX (2015) Graphene-based materials: synthesis and gas sorption, storage and separation. Prog Mater Sci 69:1–60
16. Bonaccorso F, Colombo L, Yu G et al (2015) Graphene, related two-dimensional crystals, and hybrid systems for energy conversion and storage. Science 347:1246501–1246509
17. Sun M-J, Cao X, Cao Z (2016) Si(C≡C)4-based single-crystalline semiconductor: diamond-like superlight and super flexible wide-bandgap material for the UV photoconductive device. ACS Appl Mater Interfaces 8:16551–16554
18. Chen Y, Fu K, Zhu S et al (2016) Reduced graphene oxide films with ultrahigh conductivity as Li-Ion battery current collectors. Nano Lett 16:3616–3623
19. Georgakilas V, Tiwari JN, Kemp KC et al (2016) Noncovalent functionalization of graphene and graphene oxide for energy materials, biosensing, catalytic, and biomedical applications. Chem Rev 116:5464–5519
20. Liu J, Cui L, Losic D (2013) Graphene and graphene oxide as new nanocarriers for drug delivery applications. Acta Biomater 9:9243–9257
21. Khadiran T, Hussein MZ, Zainal Z et al (2015) Activated carbon derived from peat soil as a framework for the preparation of shape-stabilized phase change material. Energy 82:468–478
22. Wu Y, Lin Y, Bol AA et al (2011) High-frequency, scaled graphene transistors on diamond-like carbon. Nature 472:74–78
23. Deng J, Li M, Wang Y (2016) Biomass-derived carbon: synthesis and applications in energy storage and conversion. Green Chem 18:4824–4854
24. Ferrari A, Robertson J (2000) Interpretation of Raman spectra of disordered and amorphous carbon. Phys Rev B 61:14095–14107
25. Wei L, Kuo PK, Thomas RL et al (1993) Thermal conductivity of isotopically modified single crystal diamond. Phys Rev Lett 70:3764–3767
26. Titirici M (2013) Sustainable carbon materials from hydrothermal processes. Wiley, Chichester, UK
27. Dai L, Chang DW, Baek J-B et al (2012) Carbon nanomaterials for advanced energy conversion and storage. Small 8:1130–1166
28. Kaneko K, Ishii C, Ruike M et al (1992) Origin of superhigh surface area and microcrystalline graphitic structures of activated carbons. Carbon 30:1075–1088
29. Pang J, Bachmatiuk A, Ibrahim I et al (2016) CVD growth of 1D and 2D sp2 carbon nanomaterials. J Mater Sci 51:640–667
30. Kroto HW, Heath JR, O'Brien SC et al (1985) C60: Buckminsterfullerene. Nature 318:162–163
31. Smalley RE (1991) Great balls of carbon: the Story of Buckminsterfullerene. The Sci 31:22–28
32. Iijima S (2002) Carbon nanotubes: past, present, and future. Phys B 323:1–5
33. Iijima S (1991) Helical microtubules of graphitic carbon. Nature 354:56–58
34. Jones DEH (1966) Hollow molecules. New Sci 32:245
35. Osawa E (1970) Superaromaticity. Kagaku (Kyoto) 25:854–863
36. Bochvar DA, Galperin EG (1973) Hypothetical systems-carbododecahedron, s-icosahedrone and carbo-s-icosahedron. Proc Acad Sci USSR 209:610–612
37. Iijima S (1980) High resolution electron microscopy of some carbonaceous materials. J Microscopy 119:99–111
38. Curl RF, Smalley RE (1991) Fullerenes. Sci Am 265:54–63
39. Iijima S, Ichihashi T (1993) Single-shell carbon nanotubes of 1-nm diameter. Nature 363:603–605
40. Bethune DS, Kiang CH, DeVries MS et al (1993) Cobalt-catalysed growth of carbon nanotubes with single-atomic-layer walls. Nature 363:605–607
41. Novoselov KS, Geim AK, Morozov SV et al (2004) Electric field effect in atomically thin carbon films. Science 306:666–669
42. Xu X, Ray R, Gu Y et al (2004) Electrophoretic analysis and purification of fluorescent single-walled carbon nanotube fragments. J Am Chem Soc 126:12736–12737

43. Pickard CJ, Needs RJ (2011) Ab initio random structure searching. J Phys Condens Matter 23:053201–053223
44. Oganov AR, Glass CW (2006) Crystal structure prediction using *ab initio* evolutionary techniques: principles and applications. J Chem Phys 124:244704–244715
45. Oganov AR, Valle M (2009) How to quantify energy landscapes of solids. J Chem Phys 130:104504–104509
46. Hautier G, Fischer C, Ehrlacher V et al (2011) Data mined ionic substitutions for the discovery of new compounds. Inorg Chem 50:656–663
47. Curtarolo S, Morgan D, Persson K et al (2003) Predicting crystal structures with data mining of quantum calculations. Phys Rev Lett 91:135503–135506
48. Fischer CC, Tibbetts KJ, Morgan D et al (2006) Predicting crystal structure by merging data mining with quantum mechanics. Nat Mater 5:641–646
49. Hautier G, Fischer CC, Jain A et al (2010) Finding nature's missing ternary oxide compounds using machine learning and density functional theory. Chem Mater 22:3762–3767
50. Meredig B, Agrawal A, Kirklin S et al (2014) Combinatorial screening for new materials in unconstrained composition space with machine learning. Phys Rev B 89:094104–094110
51. Bergerhoff G, Hundt R, Sievers R et al (1983) The inorganic crystal structure data base. J Chem Inf Comput Sci 23:66–69
52. Meredig B, Wolverton C (2013) A hybrid computational–experimental approach for automated crystal structure solution. Nat Mater 12:123–127
53. Robertson DH, Brenner DW, Mintmire JW (1992) Energetics of nanoscale graphitic tubules. Phys Rev B 45:12592–12595
54. Zhang BL, Wang CZ, Ho KM et al (1993) The geometry of large fullerene cages: C_{72} to C_{102}. J Chem Phys 98:3095–3102
55. Tang AC, Huang FQ (1995) Electronic structures of giant fullerenes with I_h symmetry. Phys Rev B 51:13830–13832
56. Dewar MJS, Thiel W (1977) Ground states of molecules. 38. The MNDO method. Approximations and parameters. J Am Chem Soc 99:4899–4907
57. Dewar MJS, Zoebisch EG, Healy EF et al (1985) J Am Chem Soc 107:3902–3909
58. Stewart JJP (1989) Optimization of parameters for semiempirical methods I. Method J Comput Chem 10:209–220
59. Dewar MJS, Jie C, Yu J (1993) SAM1; The first of a new series of general purpose quantum mechanical molecular models. Tetrahedron 49:5003–5038
60. Davidson RA (1981) Spectral analysis of graphs by cyclic automorphism subgroups. Theor Chim Acta 58:193–231
61. Schultz HP (1965) Topological organic chemistry. Polyhedranes and Prismanes. J Org Chem 30:1361–1364
62. Krätschmer W, Lamb LD, Fostiropoulos K et al (1990) Solid C60: a new form of carbon. Nature 347:354–358
63. Rohlfing EA, Cox DM, Kaldor A (1984) Production and characterization of supersonic carbon cluster beams. J Chem Phys 81:3322–3330
64. Raghavachari K, Binkley JS (1987) Structure, stability, and fragmentation of small carbon clusters. J Chem Phys 87:2191–2197
65. Parasuk V, Almolf J (1989) The electronic and molecular structure of C6: complete active space self-consistent-field and multireference configuration interaction. J Chem Phys 91:1137–1141
66. Pitzer KS, Clementi E (1959) Large molecules in carbon vapor. J Am Chem Soc 81:4477–4485
67. Hoffmann R (1966) Extended hückel theory—v: Cumulenes, polyenes, polyacetylenes and c_n. Tetrahedron 22:521–538
68. Raghavachari K, Strout DL, Odom GK et al (1993) Isomers of C20. Dramatic effect of gradient corrections in density functional theory. Chem Phys Lett 214:357–361
69. Schmalz TG, Seitz WA, Klein DJ et al (1988) Elemental carbon cages. J Am Chem Soc 110:1113–1127

70. Kroto HW (1987) The stability of the fullerenes Cn, with n = 24, 28, 32, 36, 50, 60 and 70. Nature 329:529–531
71. Taylor R, Hare JP, Abdul-sada AK et al (1990) Isolation, separation and characterisation of the fullerenes C60 and C70: the third form of carbon. J Am Chem Soc Comm 20:1423–1425
72. Ettl R, Chao I, Diederich F et al (1991) Isolation of C76, a chiral (D2) allotrope of carbon. Nature 353:149–153
73. Yan Q-L, Gozin M, Zhao F-Q et al (2016) Highly energetic compositions based on functionalized carbon nanomaterials. Nanoscale 8:4799–4851
74. Kikuchi K, Nakahara N, Wakabayashi T et al (1992) NMR characterization of isomers of C78, C82 and C84 fullerenes. Nature 357:142–145
75. Manolopoulos DE, Fowler PW, Taylor R et al (1992) Faraday communications. An end to the search for the ground state of C84? J Chem Soc Faraday Trans 88:3117–3118
76. Kadish KM, Ruoff RS (eds) (2002) Fullerene: chemistry physics and technology. Wiley, New York
77. Manolopoulos DE, Fowler PW (1992) Molecular graphs, point groups, and fullerenes. J Chem Phys 96:7603–7614
78. Shustova NB, Kuvychko IV, Bolskar RD et al (2006) Trifluoromethyl Derivatives of Insoluble Small-HOMO−LUMO-Gap Hollow Higher Fullerenes. NMR and DFT Structure Elucidation of C_2-(C_{74}–D_{3h})(CF_3)$_{12}$, C_s-(C_{76}-T_d(2))(CF_3)$_{12}$, C_2-(C_{78}–D_{3h}(5))(CF_3)$_{12}$, C_s-(C_{80}–C_{2v}(5))(CF_3)$_{12}$, and C_2-(C_{82}–C_2(5))(CF_3)$_{12}$. J Am Chem Soc 128:15793–15798
79. Shustova NB, Newell BS, Miller SM et al (2007) Discovering and verifying elusive fullerene cage isomers: structures of C_2–p^{11}-(C_{74}–D_{3h})(CF_3)$_{12}$ and C_2–p^{11}-(C_{78}–D_{3h}(5))(CF_3)$_{12}$. Angew Chem 46:4111–4114
80. Amsharov KY, Jensen M (2008) A C_{78} fullerene precursor: toward the direct synthesis of higher fullerenes. J Org Chem 73:2931–2934
81. Manolopoulos DE, Fowler PW (1991) Structural proposals for endohedral metal—fullerene complexes. Chem Phys Lett 187:1–7
82. Shao N, Gao Y, Yoo S et al (2006) Search for lowest-energy fullerenes: C_{98} to C_{110}. J Phys Chem A 110:7672–7676
83. Shao N, Gao Y, Zeng XC (2007) Search for lowest-energy fullerenes 2: C_{38} to C_{80} and C_{112} to C_{120}. J Phys Chem C 111:17671–17677
84. Slanina Z, Uhlik F, Yoshida M et al (2000) A computational treatment of 35 IPR isomers of C_{88}. Fullerene Sci Technol 8:417–432
85. Slanina Z, Zhao X, Deota P et al (2000) Relative stabilities of C_{92} IPR fullerenes. J Mol Model 6:312–317
86. Sun G (2003) Assigning the major isomers of fullerene C_{88} by theoretical ^{13}C NMR spectra. Chem Phys Lett 367:26–33
87. Sun G, Kertesz M (2002) ^{13}C NMR spectra for IPR isomers of fullerene C_{86}. Chem Phys 276:107–114
88. Zhao X, Slanina Z, Goto H (2004) Theoretical studies on the relative stabilities of C_{96} IPR fullerenes. J Phys Chem A 108:4479–4484
89. Zhao X, Goto H, Slanina Z (2004) C100 IPR fullerenes: temperature-dependent relative stabilities based on the Gibbs function. Chem Phys 306:93–104
90. Fowler PW, Steer JI (1987) The leapfrog principle: a rule for electron counts of carbon clusters. J Chem Soc Chem Commun 9:1403–1405
91. Amic D, Trinajstic N (1990) On the lack of reactivity of Buckminsterfullerene. A theoretical study. J Chem Soc Perkin Trans 2:1595–1598
92. Coulombeau C, Rassat A (1987) Calculs de propriétés électroniques et des fréquences normales de vibration d'agrégats carbonés formant des polyèdres réguliers et semi-réguliers. J Chim Phys 84:875–882
93. Ozaki M, Takahashi A (1986) On electronic states and bond lengths of the truncated icosahedral C60 molecule. Chem Phys Lett 127:242–244
94. Liithi HP, Almlof J (1987) AB initio studies on the thermodynamic stability of the icosahedral C60 molecule "buckminsterfullerene." Chem Phys Lett 135:357–360

95. Almlof J, Luthi HP (1987) Theoretical methods and results for electronic structure calculations on very large systems. ACS Symp. Ser. 353: (Supercomut. Res. Chem. Chem. Eng.), 35–48
96. Almlof J (1990) Carbon in the Galaxy. In: Tarter JC, Chang S, DeFrees DJ (eds) National Aeronautics and Space Administration Conference Publication Washington, DC, 1990, vol 3061. NASA, USA, p 245
97. Schulman JM, Disch RL (1991) The heat of formation of buckminsterfullerene, C60. J Chem Soc Chem Comm 6:411–412
98. Larsson S, Volosov A (1987) Rosen A (1987) Optical spectrum of the icosahedral C60-"follene-60." Chem Phys Lett 137:501–504
99. Braga M, Larsson S, Rosen A et al (1991) Electronic transition in C60—on the origin of the strong interstellar absorption at 217 NM. Astron Astrophys 245:232–238
100. Kataoka M, Nakajima T (1986) Geometrical structures and spectra of corannulene and icosahedral C_{60}. Tetrahedron 42:6437–6442
101. Lazlo I, Udvardi L (1987) On the geometrical structure and UV spectrum of the truncated icosahedral C60, molecule. Chem Phys Lett 136:418–422
102. Hayden GW, Mele EJ (1987) π bonding in the icosahedral C60 cluster. Phys Rev B 36:5010–5015
103. Newton MD, Stanton RE (1986) Stability of buckminsterfullerene and related carbon clusters. J Am Chem Soc 108:2469–2470
104. Elser V, Haddon RC (1987) Icosahedral C60: an aromatic molecule with a vanishingly small ring current magnetic susceptibility. Nature 325:792–794
105. Elser V, Haddon RC (1987) Magnetic behavior of icosahedral Csub60. Phys Rev A 36:4579–4584
106. Fowler PW, Lazzeretti P, Zanasi R (1990) Electric and magnetic properties of the aromatic sixty-carbon cage. Chem Phys Lett 165:79–86
107. Haddon RC, Elser V (1990) Icosahedral C60 revisited: an aromatic molecule with a vanishingly small ring current magnetic susceptibility. Chem Phys Lett 169:362–364
108. Schmalz TG (1990) The magnetic susceptibility of Buckminsterfullerene. Chem Phys Lett 175:3–5
109. Dresselhaus MS, Dresselhaus G, Eklund PC (1996) Science of fullerenes and carbon nanotubes: their properties and applications. Elsevier, San Diego
110. Lebedeva MA, Chamberlain TW, Khlobystov AN (2015) Harnessing the synergistic and complementary properties of fullerene and transition-metal compounds for nanomaterial applications. Chem Rev. 115:11301–11351
111. Lim SY, Shen W, Gao Z (2015) Carbon quantum dots and their applications. Chem Soc Rev 44:362–381
112. Zhu S, Song Y, Zhao X et al (2015) The photoluminescence mechanism in carbon dots (graphene quantum dots, carbon nanodots, and polymer dots): current state and future perspective. Nano Res 8:355–381
113. Baker SN, Baker GA (2010) Luminescent carbon nanodots: emergent nanolights. Angew Chem Int Ed. 49:6726–6744
114. Sun Y-P, Zhou B, Lin Y et al (2006) Quantum-sized carbon dots for bright and colorful photoluminescence. J Am Chem Soc 128:7756–7757
115. Yamijala SSRKC, Bandyopadhyay A, Pati SK (2014) Electronic properties of zigzag, armchair and their hybrid quantum dots of graphene and boron-nitride with and without substitution: A DFT study. Chem Phys Lett 603:28–32
116. Saidi WA (2013) Oxygen reduction electrocatalysis using N-Doped graphene quantum-dots. J Phys Chem Lett 4:4160–4165
117. Kumar GS, Roy R, Sen D et al (2014) Amino-functionalized graphene quantum dots: origin of tunable heterogeneous photoluminescence. Nanoscale 6:3384–3391
118. Zhao M, Yang F, Xue Y et al (2014) A time-dependent DFT study of the absorption and fluorescence properties of graphene quantum dots. Chem Phys Chem 15:950–957
119. Sk MA, Ananthanarayanan A, Huang L et al (2014) Revealing the tunable photoluminescence properties of graphene quantum dots. J Mater Chem C 2:6954–6960

120. Zarenia M, Chaves A, Farias GA et al (2011) Energy levels of triangular and hexagonal graphene quantum dots: a comparative study between the tight-binding and Dirac equation approach. Phys Rev B 84:245403–245414
121. Li H, He X, Kang Z et al (2010) Water-soluble fluorescent carbon quantum dots and photocatalyst design. Angew Chem Int Ed 49:4430–4434
122. Choudhary RP, Shukla S, Vaibhav K et al (2015) Optical properties of few layered graphene quantum dots. Mater Res Express 2:095024–095028
123. Zhang RQ, Bertran E, Lee S-T (1998) Size dependence of energy gaps in small carbon clusters: the origin of broadband luminescence. Diamond Relat Mater 7:1663–1668
124. Zhu B, Sun S, Wang Y et al (2013) Preparation of carbon nanodots from single chain polymeric nanoparticles and theoretical investigation of the photoluminescence mechanism. J Mater Chem C 1:580–586
125. Park Y, Yoo J, Lim B et al (2016) Improving the functionality of carbon nanodots: doping and surface functionalization. J Mater Chem A 4:11582–11603
126. Hu S, Tian R, Wu L et al (2013) Chemical regulation of carbon quantum dots from synthesis to photocatalytic activity. Chem Asian J 8: 1035–1041
127. Kwon W, Do S, Kim J-H et al (2015) Control of Photoluminescence of carbon nanodots via surface functionalization using para-substituted anilines. Sci Rep 5:12604–12613
128. Margraf JT, Strauss V, Guldi DM et al (2015) The electronic structure of amorphous carbon nanodots. J Phys Chem B 119:7258–7265
129. Ajayan PM, Stephan O, Colliex C et al (1994) Aligned carbon nanotube arrays formed by cutting a polymer resin—nanotube composite. Science 265:1212–1214
130. Saito Y, Hamaguchi K, Hata K et al (1997) Conical beams from open nanotubes. Nature 389:554–555
131. de Heer WA, Châtelain A, Ugarte D (1995) A carbon nanotube field-emission electron source. Science 270:1179–1180
132. Collins PG, Zettl A, Bando H et al (1997) Nanotube nanodevice. Science 278:100–102
133. Nardelli MB, Yakobson BI, Bernholc J (1998) Mechanism of strain release in carbon nanotubes. Phys Rev B 57:R4277-4280
134. Huang JY, Chen S, Ren ZF et al (2006) Real-time observation of tubule formation from amorphous carbon nanowires under high-bias joule heating. Nano Lett 6:1699–1705
135. Radushkevich LV, Lukyanovich VM (1952) The structure of carbon forming in thermal decomposition of carbon monoxide on an iron catalyst. Russian J Phys Chem 26:88–95
136. Saxena S, Tyson TA (2010) Ab initio density functional studies of the restructuring of graphene nanoribbons to form tailored single walled carbon nanotubes. Carbon 48:1153–1158
137. Saito R, Dresselhaus G, Dresselhaus MS (1998) Physical properties of carbon nanotubes. Press, London, Imp. Coll
138. Terrones M (2003) Science and technology of the twenty-first century: synthesis, properties, and applications of carbon nanotubes. Ann Rev Mater Res 33:419–501
139. Zhang M, Li J (2009) Carbon nanotube in different shapes. Mater Today 12:12–18
140. Elliott JA, Sandler JKW, Windle AH et al (2004) Collapse of single-wall carbon nanotubes is diameter dependent. Phys Rev Lett 92:095501–095504
141. Ebbesen TW, Lezec HJ, Hiura H et al (1996) Electrical conductivity of individual carbon nanotubes. Nature 382:54–56
142. Saito R, Fujita M, Dresselhaus G et al (1992) Electronic structure of chiral graphene tubules. Appl Phys Lett 60:2204–2206
143. Delaney P, Di Ventra M, Pantelides ST (1999) Quantized conductance of multiwalled carbon nanotubes. Appl Phys Lett 75:3787–3789
144. Yu MF, Lourie O, Dyer MJ et al (2000) Strength and breaking mechanism of multiwalled carbon nanotubes under tensile load. Science 287:637–640
145. Yu MF, Files BS, Arepalli S et al (2000) Tensile loading of ropes of single wall carbon nanotubes and their mechanical properties. Phys Rev Lett 84:5552–5555
146. Xie S, Li W, Pan Z et al (2000) Mechanical and physical properties on carbon nanotube. J Phys Chem Solids 61:1153–1158

147. Overney G, Zhong W, Tomanek D (1993) Structural rigidity and low frequency vibrational modes of long carbon tubules. Z Phys D 27:93–96
148. Tersoff J (1992) Energies of fullerenes. Phys Rev B 46:15546–15549
149. Sinnott SB, Shenderova OA, White CT et al (1998) Mechanical properties of nanotubule fibers and composites determined from theoretical calculations and simulations. Carbon 36:1–9
150. Yakobson BI (1998) Mechanical relaxation and "intramolecular plasticity" in carbon nanotubes. Appl Phys Lett 72:918–920
151. Ru CQ (2000) Effect of van der Waals forces on axial buckling of a double-walled carbon nanotube. J Appl Phys 87:7227–7231
152. Saxena S, Tyson TA (2010) Interacting quasi-two-dimensional sheets of interlinked carbon nanotubes: a high-pressure phase of carbon. ACS Nano 4:3515–3521
153. Gao G, Çagin T, Goddard WA III (1998) Energetics, structure, mechanical and vibrational properties of single-walled carbon nanotubes. Nanotechnology 9:184–191
154. Hernandez E, Goze C, Bernier P et al (1998) Elastic properties of C and BxCyNz composite nanotubes. Phys Rev Lett 80:4502–4505
155. Yu M-F, Kowalewski T, Ruoff RS (2000) Investigation of the radial deformability of individual carbon nanotubes under controlled indentation force. Phys. Rev. Lett. 85:1456–1459
156. Saeed K, Khan I (2013) Carbon nanotubes–properties and applications: a review. Carbon Lett 14:131–144
157. Ruoff RS, Lorents DC (1995) Mechanical and thermal properties of carbon nanotubes. Carbon 33:925–930
158. Ashcroft NW (1976) Mermin N D (1976) Solid State Physics. Harcourt Brace, Orlando, FL
159. Kim P, Shi L, Majumdar A et al (2001) Thermal transport measurements of individual multiwalled nanotubes. Phys Rev Lett 87:215502–215505
160. Yu C, Shi L, Yao Z et al (2005) Thermal conductance and thermopower of an individual single-wall carbon nanotube. Nano Lett 5:1842–1846
161. Maultzsch J, Reich S, Thomsen C et al (2002) Phonon dispersion of carbon nanotubes. Solid State Commun 121:471–474
162. Ishii H, Kobayashi N, Hirose K (2007) Electron–phonon coupling effect on quantum transport in carbon nanotubes using time-dependent wave-packet approach. Phys E 40:249–252
163. Maeda T, Horie C (1999) Phonon modes in single-wall nanotubes with a small diameter. Phys B 263–264:479–481
164. Kasuya A, Saito Y, Sasaki Y et al (1996) Size dependent characteristics of single wall carbon nanotubes. Mater Sci Eng A 217–218:46–47
165. Popov VN (2004) Theoretical evidence for $T^{1/2}$ specific heat behavior in carbon nanotube systems. Carbon 42:991–995
166. Segal M (2012) Material history: learning from silicon. Nature 483:S43–S44
167. Falcao EHL, Wudl F (2007) Carbon allotropes: beyond graphite and diamond. J Chem Technol Biotechnol 82:524–531
168. Aristov VY, Urbanik G, Kummer K et al (2010) Graphene synthesis on cubic SiC/Si wafers. perspectives for mass production of graphene-based electronic devices. Nano Lett 10:992–995
169. Hernandez Y, Nicolosi V, Lotya M et al (2008) High-yield production of graphene by liquid-phase exfoliation of graphite. Nat Nanotechnol 3:563–568
170. Paredes JI, Villar-Rodil S, Fernández-Merino MJ et al (2011) Environmentally friendly approaches toward the mass production of processable graphene from graphite oxide. J Mater Chem 21:298–306
171. Dikin DA, Stankovich S, Zimney EJ et al (2007) Preparation and characterization of graphene oxide paper. Nature 448:457–460
172. Wang G, Yang J, Park J et al (2008) Facile synthesis and characterization of graphene nanosheets. J Phys Chem C 112:8192–8195
173. Prasai D, Tuberquia JC, Harl RR et al (2012) Graphene: corrosion-inhibiting coating. ACS Nano 6:1102–1108
174. Kiran SK, Shukla S, Struck A et al (2019) Surface enhanced 3D rGO hybrids and porous rGO nano-networks as high performance supercapacitor electrodes for integrated energy storage devices. Carbon 158:527–535

175. Kiran SK, Shukla S, Struck A et al (2019) Surface engineering of graphene oxide shells using Lamellar LDH nanostructures. ACS Appl Mater Interfaces 11:20232–20240
176. Zhao X, Hayner CM, Kung MC et al (2011) In-plane vacancy-enabled high-power Si–graphene composite electrode for Lithium-Ion batteries. Adv Energy Mater 1:1079–1084
177. Z. Radivojevic, et al. (2012) Electrotactile touch surface by using transparent graphene. In: VRIC '12: proceedings of the 2012 virtual reality international conference, association for computing machinery, New York, NY, USA
178. Wang H, Sun K, Tao F et al (2013) 3D honeycomb-like structured graphene and its high efficiency as a counter-electrode catalyst for dye-sensitized solar cells. Angew Chem Int Ed Engl 52:9210–9214
179. Pawar PB, Saxena S, Bhade DK et al (2016) 3D oxidized graphene frameworks for efficient nano sieving. Sci Rep 6:21150–21154
180. Shejale KP, Yadav D, Patil H et al (2020) Evaluation of techniques for the remediation of antibiotic-contaminated water using activated carbon. Mol Syst Des Eng 5:743–756
181. Pandey A, Deb M, Tiwari S et al (2018) 3D oxidized graphene frameworks: an efficient adsorbent for methylene blue. J Mater 70:469–472
182. Pawar PB, Maurya SK, Chaudhary RP et al (2016) Water purification using graphene covered micro-porous, reusable carbon membrane. MRS Adv 1:1411–1416
183. Wallace PR (1947) The band theory of graphite. Phys Rev 71:622–634
184. Slater JC, Koster GF (1954) Simplified LCAO method for the periodic potential problem. Phys Rev B 94:1498–1524
185. Harrison (1980) Electronic structure and the properties of solids: the physics of the chemical bond. W. H, Freeman and Company, San Francisco, p 1980
186. Boehm HP, Clauss A, Fisher GO et al (1962) Das Adsorptionsverhalten sehr dünner Kohlenstoff-Folien. Zeitschrift Fur Anorg Und Allg Chemie 316:119–127
187. Fuhrer MS, Lau CN, MacDonald AH (2010) Graphene: materially better carbon. MRS Bull 35:289–295
188. Singh V, Joung D, Zhai L et al (2011) Graphene based materials: past, present and future. Prog Mater Sci 56:1178–1271
189. Kim KS, Zhao Y, Jang H et al (2009) Large-scale pattern growth of graphene films for stretchable transparent electrodes. Nature 457:706–710
190. Balandin AA, Ghosh S, Bao W et al (2008) Superior thermal conductivity of single-layer graphene. Nano Lett 8:902–907
191. Lee C, Wei X, Kysar JW et al (2008) Measurement of the elastic properties and intrinsic strength of monolayer graphene. Science 321:385–388
192. Zhu Y, Murali S, Cai W et al (2010) Graphene and graphene oxide: synthesis, properties, and applications. Adv Mater 22:3906–3924